DALTON
FULL PAPER

N–N Bridged dinuclear complexes with Mn(II), Ni(II), Cu(II), Zn(II) and Cd(II); examples with antiferromagnetic and ferromagnetic coupling

Zhiqiang Xu,[a] Laurence K. Thompson,*[a] Daniel A. Black,[a] Corbin Ralph,[a] David O. Miller,[a] Michael A. Leech[b] and Judith A. K. Howard[b]

[a] *Department of Chemistry, Memorial University of Newfoundland, St. John's, Newfoundland, A1B 3X7, Canada*
[b] *Department of Chemistry, University of Durham, Durham, UK DH1 3LE*

Received 14th February 2001, Accepted 11th May 2001
First published as an Advance Article on the web 11th June 2001

A series of new complexes of some bis-bidentate N_4 ligands [picolinamide azine (pahap), 2-pyrazinecarboxamide azine (pzhpz) and butanedione-monoxime picolinamide hydrazone (pahox)], based on a rotationally flexible N–N bridging unit, with Mn(II), Ni(II), Cu(II), Zn(II) and Cd(II) is reported. 2 : 2 (M : L) ratio complexes with Mn(II) and Cd(II), in which anionic ligands (Cl^-, NO_3^-) are bonded to the metals, have large >80° M–N–N–M torsional angles, indicating 'open' dinuclear structures. With weakly or non-coordinating anions (*e.g.* ClO_4^-, $ZnBr_4^{2-}$) 2 : 3 complexes are formed with smaller torsional angles (39–43°) in keeping with the presence of three N–N bridges and 'closed' spiral structures. Antiferromagnetic exchange is observed bewteen Mn(II) and Ni(II) centres in both types of complex, whereas with Cu(II) small Cu–N–N–Cu angles lead to dominant ferromagnetic exchange coupling. Structural and magnetic data are discussed.

Introduction

The bis-bidentate ligands pahap (picolinamide azine, see Scheme 1) and pahox (butanedione-monoxime picolinamide

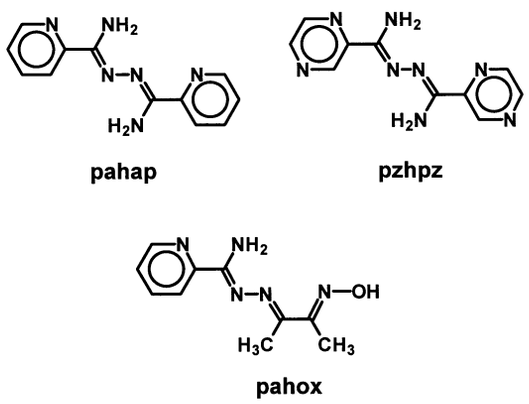

Scheme 1

hydrazone) exhibit rotational flexibility around the N–N bond, and have been shown to produce twisted mono-ligand and di-ligand dinuclear complexes with Cu(II) with N–N single bond bridges between the metal centres. Magnetic properties depend on the angle of rotation of the copper magnetic planes around the N–N bond, and relative orientation of the nitrogen p orbitals.[1–3] Acute angles (< 80°) lead to ferromagnetic coupling, while at larger angles antiferromagnetic coupling is observed, with a linear relationship between exchange integral and angle. The related dipyrazine ligand pzhpz (2-pyrazinecarboxamide azine) behaves in a similar manner. Pahap and pzhpz also form spiral dinuclear complexes $[M_2L_3]X_4$ (L = pahap; M = Mn(II), X = ClO_4^-, M = Fe(II), X = NO_3^-, M = Co(III), X = NO_3^-, M = Ni(II), X = NO_3^-; L = pzhpz; M = Fe(II), X = NO_3^-) in which three ligands wrap themselves around the dinuclear center with the N–N diazine fragments acting as the bridges. The spiral conformations of these tris-ligand complexes are effectively locked in place, with small M–N–N–M torsional angles, leading either to weak antiferromagnetic or ferromagnetic coupling.[4] The present study describes a series of new dinuclear di-ligand and tri-ligand complexes with the ligands pahap, pzhpz and pahox, again involving just single N–N bridges between the metal centres (metal = Mn(II), Ni(II), Cu(II), Zn(II), Cd(II)). Magnetic properties indicate weak antiferromagnetic coupling or no coupling for the manganese and nickel complexes, and ferromagnetic coupling for the copper derivatives.

Experimental

Materials

Commercially available solvents and chemicals were used without further purification.

Physical measurements

Electronic spectra were recorded as Nujol mulls and in solution using a Cary 5E spectrometer. Infrared spectra were recorded as Nujol mulls using a Mattson Polaris FTIR instrument. Mass spectra were obtained using a VG micromass 7070HS spectrometer. C, H, N analyses on vacuum dried samples (24 h) were performed by the Canadian Microanalytical Service, Delta, BC, Canada. Variable temperature magnetic data (2–300 K) were obtained with a Quantum Design MPMS5S Squid magnetometer operating at 0.1–0.5 T. Calibrations were carried out with a palladium standard cylinder, and temperature errors were determined with $[H_2tmen][CuCl_4]$ (H_2tmen = $(CH_3)_2HNCH_2CH_2NH(CH_3)_2^{2+}$).[5]

Preparations

Pahap, pzhpz and pahox were prepared by procedures described in previous reports.[1,2,4]

$[Mn_2(pahox)_2Cl_4]\cdot H_2O$ ($1\cdot H_2O$). Pahox (0.22 g, 1.0 mmol) was added to a warm aqueous methanol (4 : 1) solution (25

 DOI: 10.1039/b101445p

mL) of $MnCl_2·6H_2O$ (3.0 mmol, 0.70 g) and the mixture stirred for several minutes until the ligand dissolved. The clear solution was filtered and the filtrate allowed to stand at room temperature for two days. Well formed orange crystals were produced, which were filtered off, washed with cold water, and dried in air (Yield 83%). (Found: C, 33.81; H, 3.88; N, 19.57. $[Mn_2(C_{10}H_{13}N_5O)_2Cl_4]·H_2O$ requires: C, 33.92; H, 3.98; N, 19.78%). ν_{max}/cm^{-1}: 3350 (=NOH), 3308, 3161(NH), 1643 (C=N) and 1046, 1015 (py) (Nujol).

$[Ni_2(pahox)_3](ClO_4)_4·4H_2O$ (2·4H$_2$O). This compound was prepared as red-brown crystals in a similar manner to compound **1** (Yield 92%). (Found: C, 28.93; H, 3.66; N, 16.58. $[Ni_2(C_{10}H_{13}N_5O)_3](ClO_4)_4·4H_2O$ requires: C, 28.94; H, 3.85; N, 16.87%). λ_{max}/nm (Nujol): 420, 540, 840(sh), 900. ν_{max}/cm^{-1}: 3515 (H_2O), 3423 (=NOH), 3348, 3215 (NH), 1657 (C=N), 1098, 620 (ClO_4^-) and 1048 (py) (Nujol).

$[Ni_2(pzhpz)_3](ClO_4)_4·4H_2O$ (3·4H$_2$O). *Method A.* Compound **4** (0.67 g, 0.50 mmol) was dissolved in 20 mL hot water to give a clear yellow-green solution. $Ni(en)_2Cl_2·H_2O$ (0.81 g, 1.5 mmol), pre-dissolved in 5 mL water, was added to this solution with stirring. A clean red-orange solution was obtained, which was filtered, and the filtrate allowed to stand for several days at room temperature. Red-orange crystals, suitable for structural analysis, were collected (Yield 75% referred to compound **4**). (Found: C, 27.47; H, 2.72; N, 25.55. $[Ni_2(C_{10}H_{10}N_8)_3](ClO_4)_4·4H_2O$ requires: C, 27.42; H, 2.91; N, 25.58%). λ_{max}/nm (Nujol): 425, 545, 843(sh), 900. ν_{max}/cm^{-1}: 3585 (H_2O), 3370, 3167 (NH), 1658 (C=N) and 1080, 625 (ClO_4^-) (Nujol).

Method B. This compound can be produced from the direct reaction of pzhpz with $Ni(ClO_4)_2·6H_2O$ in water with higher yield (over 90%). However, it is always in powdered form.

$[Cu_2(pzhpz)_3](ClO_4)_4·5H_2O$ (4·5H$_2$O). Pzhpz (0.73 g, 3.0 mmol) was suspended in a hot, stirred aqueous solution of $Cu(ClO_4)_2·6H_2O$ (0.36 g, 1.0 mmol in 20 mL deionized water). 10 mL of methanol was added forming a clear light green solution after a few minutes. Another 1.0 mmol of $Cu(ClO_4)_2·6H_2O$ (dissolved in 5 mL of deionized water) was added to the resulting solution, forming a deeper green solution. The solution was filtered and allowed to stand at room temperature for a few hours. Green crystals, suitable for structural analysis, formed (Yield 90%). (Found: C, 26.98; H, 2.80; N, 25.23. $[Cu_2(C_{10}H_{10}N_8)_3](ClO_4)_4·5H_2O$ requires: C, 26.86; H, 3.00; N, 25.06%). λ_{max}/nm (Nujol): 720. ν_{max} /cm^{-1}: 3592 (H_2O), 3368, 3165 (NH), 1657 (C=N) and 1080, 625 (ClO_4^-) (Nujol).

$[Cu_2(pahap)_3](ClO_4)_4·5H_2O$ (5·5H$_2$O). This compound was prepared as light green crystals in a similar manner to compound **4** (Yield 89%). (Found: C, 32.32; H, 3.24; N, 18.79. $[Cu_2(C_{12}H_{12}N_6)_3](ClO_4)_4·5H_2O$ requires: C, 32.37; H, 3.47; N, 18.87%). λ_{max}/nm (Nujol): 690. ν_{max} /cm^{-1}: 3571 (H_2O), 3390, 3315, 3167 (NH), 1656 (C=N), 1094, 626 (ClO_4^-) and 1048 (py) (Nujol).

$[Zn_2(pahap)_3](ZnBr_4)_2·5H_2O$ (6·5H$_2$O). Pahap (0.24 g, 1.0 mmol) was added to an aqueous solution (20 mL) of $ZnBr_2·6H_2O$ (0.67 g, 2.0 mmol), and the mixture was stirred for several minutes at room temperature until the ligand dissolved. The colorless solution was filtered, and the filtrate was allowed to stand at room temperature for several days. Very light yellow (almost colorless) crystals, suitable for an X-ray structural determination, formed. These were filtered off, washed quickly with water and air-dried (Yield 79%). (Found: C, 25.33; H, 2.50; N, 14.70. $[Zn_2(C_{12}H_{12}N_6)_3](ZnBr_4)_2·5H_2O$ requires: C, 25.26; H, 2.71; N, 14.73%). ν_{max}/cm^{-1}: 3550(br) (H_2O), 3303, 3165 (NH), 1656 (C=N) and 1017 (py) (Nujol).

$[Cd_2(pahap)_2(NO_3)_2(H_2O)_2](NO_3)_2·4H_2O$ (7·4H$_2$O). This compound was synthesized as white crystals in a similar manner to compound **6**, using $Cd(NO_3)_2·6H_2O$ (Yield 90%). (Found: C, 27.00; H, 3.45; N, 21.10. $[Cd_2(C_{12}H_{12}N_6)_2(NO_3)_2(H_2O)_2](NO_3)_2·4H_2O$ requires: C, 27.16; H, 3.42; N, 21.11%). ν_{max}/cm^{-1}: 3550, 3520 (H_2O), 3360, 3185 (NH), 1665 (C=N), 1765 and 1755 ($\nu_1 + \nu_4$ monodentate and ionic NO_3^-), and 1020 (py) (Nujol).

CAUTION: although no problems were encountered with the perchlorate complexes reported in this study, readers are cautioned about the potentially explosive nature of such compounds.

Crystallography

Crystal data and information about the data collections and structural refinements are summarized in Table 1.

The diffraction intensities of single crystals of **1**, **6** and **7** were collected with graphite monochromated Mo-Kα X-radiation and **2** with Cu-Kα radiation using a Rigaku AFC6S diffractometer at 299(1) K and the ω–2θ scan technique. The data were corrected for Lorentz and polarization effects. The structures were solved by direct methods.[6,7] All atoms except hydrogens were refined anisotropically for **1**, **2**, **6** and **7** unless otherwise stated. Hydrogen atoms were optimized by positional refinement, with isotropic thermal parameters set 20% greater than those of their bonded partners at the time of their inclusion. However they were fixed for the final round of refinement. Neutral atom scattering factors[8] and anomalous-dispersion terms[9,10] were taken from the usual sources. All calculations were performed with the teXsan[11] crystallographic software package using a PC computer. For **2** significant disorder in three of the lattice perchlorates prevented a good refinement of the structure. The disorder could not be modeled in a systematic way, and oxygen atoms from these perchlorates and lattice water molecules were refined isotropically. For **6** three oxygen atoms of the partially occupied water molecules were refined isotropically, and one half occupancy hydrogen atom was not found.

The diffraction intensities of a single crystal of **3** were collected with graphite monochromatized Mo-Kα X-radiation (rotating anode generator) using a Bruker P4/CCD diffractometer at 193(1) K to a maximum 2θ value of 51.5°. The data were treated and the structure solved as before using teXsan. Abbreviated crystal data for **3** are given in Table 1.

Diffraction data for a single crystal of **4** were collected using a Bruker SMART CCD diffractometer, equipped with an Oxford Cryostream N_2 cooling device,[12] with graphite monochromated Mo-Kα radiation. Cell parameters were determined and refined using the SMART software,[13a] raw frame data were integrated using the SAINT program,[13b] and the structure was solved using direct methods and refined by full-matrix least squares on F^2 using SHELXTL.[14] Non-hydrogen atoms were refined with anisotropic atomic displacement parameters (adps).

CCDC reference numbers 158599–158604.

See http://www.rsc.org/suppdata/dt/b1/b101445p/ for crystallographic data in CIF or other electronic format.

Results and discussion

Stuctures

Crystal structure of $[Mn_2(pahox)_2Cl_4]·H_2O$ (1·H$_2$O). The structure of **1** is shown in Fig. 1, and selected bond distances and angles are listed in Table 2. The neutral complex consists of two ligands straddling the two six-coordinate metals in axial positions, in a pseudo-*cis* fashion, with N–N single bond bridges. Two chlorine atoms act as weak terminal equatorial ligands (Mn–Cl 2.44–2.47 Å). Three Mn–N distances per metal

Table 1 Summary of crystallographic data for $[Mn_2(pahox)_2Cl_4]\cdot H_2O$ (**1**·H_2O), $[Ni_2(pahox)_3](ClO_4)_4\cdot 4H_2O$ (**2**·$4H_2O$),$[Ni_2(pzhpz)_3](ClO_4)_4\cdot 4H_2O$ (**3**·$4H_2O$), $[Cu_2(pzhpz)_3](ClO_4)_4\cdot 5H_2O$ (**4**·$5H_2O$), $[Zn_2(pahap)_3](ZnBr_4)_2\cdot 5H_2O$ (**6**·$5H_2O$) and $[Cd_2(pahap)_2(NO_3)_2(H_2O)_2](NO_3)_2\cdot 4H_2O$ (**7**·$4H_2O$)

Compound	**1**	**2**	**3**	**4**	**6**	**7**
Empirical formula	$C_{20}H_{26}N_{10}O_2Cl_4Mn_2$	$C_{30}H_{46.3}N_{15}O_{22.65}Cl_4Ni_2$	$C_{30}H_{41.5}N_{24}O_{21.75}Cl_4Ni_2$	$C_{30}H_{40}N_{24}O_{21}Cl_4Cu_2$	$C_{36}H_{43}N_{18}Br_8O_{3.5}Zn_4$	$C_{24}H_{38}N_{16}O_{19}Cd_2$
Formula weight	690.18	1238.69	1345.52	1341.7	1684.61	1079.48
Space group	*Pna*21 (no. 33)	$P2_1/n$ (no. 14)	$P2_1/c$ (no. 14)	$P2_1/c$	$P\bar{1}$	$C2/c$ (no. 15)
a/Å	24.219(5)	19.277(5)	17.6681(11)	17.7623(8)	16.088(2)	23.870(3)
b/Å	9.127(2)	21.233(5)	13.3204(8)	13.3002(6)	16.950(4)	13.418(8)
c/Å	13.515(2)	12.479(3)	22.0456(13)	21.6942(10)	11.104(3)	14.721(5)
α/°					108.37(2)	
β/°		98.20(2)	90.343(1)	90.3990(10)	101.84(2)	119.90(1)
γ/°					90.75(2)	
V/Å^3	2987.6(9)	5055(2)	5188.3(5)	5125.0(4)	2803(1)	4087(2)
ρ_{calc}/g cm^{-3}	1.534	1.627	1.722	1.739	1.996	1.754
Z	4	4	4	4	2	4
μ/cm^{-1}	12.39	36.96	10.33	11.4	74.64	11.36
λ/Å	0.71069	1.54178	0.71073	0.71073	0.71069	0.71069
T/°C	26(1)	26(1)	−80(1)	−173(1)	26(1)	26(1)
R	0.034	0.110	0.041(R_1)	0.0277(R_1)	0.048	0.037
R_w	0.028	0.112	0.122(wR_2)	0.0733(wR_2)	0.047	0.039

[a] $R = \Sigma||F_o| - |F_c||/\Sigma|F_o|$, $R_w = \{[\Sigma w(|F_o| - |F_c|)^2/\Sigma wF_o^2]\}^{1/2}$. [b] $R_1 = \Sigma||F_o| - |F_c||/\Sigma|F_o|$, $wR_2 = \{\Sigma[w(|F_o|^2 - |F_c|^2)^2]/\Sigma[w(|F_o|^2)^2]\}^{1/2}$.

Table 2 Distances (Å) and angles (°) for **1**

Mn(1)–Cl(1)	2.45(1)	Mn(2)–N(4)	2.357(5)
Mn(1)–Cl(2)	2.449(2)	Mn(2)–N(5)	2.271(9)
Mn(1)–N(1)	2.284(8)	Mn(2)–N(6)	2.273(9)
Mn(1)–N(3)	2.259(9)	Mn(2)–N(8)	2.294(6)
Mn(1)–N(9)	2.464(8)	Mn(1)–Mn(2)	4.821(3)
Mn(1)–N(10)	2.272(8)	N(3)–N(4)	1.411(5)
Mn(2)–Cl(3)	2.464(4)	N(8)–N(9)	1.41(1)
Mn(2)–Cl(4)	2.446(7)		
Cl(1)–Mn(1)–Cl(2)	102.6(3)	Cl(3)–Mn(2)–Cl(4)	99.8(3)
Cl(1)–Mn(1)–N(1)	95.4(2)	Cl(3)–Mn(2)–N(5)	83.3(2)
Cl(1)–Mn(1)–N(3)	106.6(2)	Cl(3)–Mn(2)–N(6)	91.2(3)
Cl(1)–Mn(1)–N(10)	83.7(3)	Cl(3)–Mn(2)–N(8)	103.0(1)
Cl(2)–Mn(1)–N(1)	88.9(2)	Cl(4)–Mn(2)–N(5)	92.0(2)
Cl(2)–Mn(1)–N(3)	145.6(5)	Cl(4)–Mn(2)–N(6)	92.3(3)
Cl(2)–Mn(1)–N(10)	89.6(2)	Cl(4)–Mn(2)–N(8)	152.0(1)
N(1)–Mn(1)–N(3)	70.7(3)	N(5)–Mn(2)–N(6)	173.5(1)
N(1)–Mn(1)–N(10)	178.0(3)	N(5)–Mn(2)–N(8)	106.6(4)
N(3)–Mn(1)–N(10)	111.2(2)	N(6)–Mn(2)–N(8)	71.3(3)

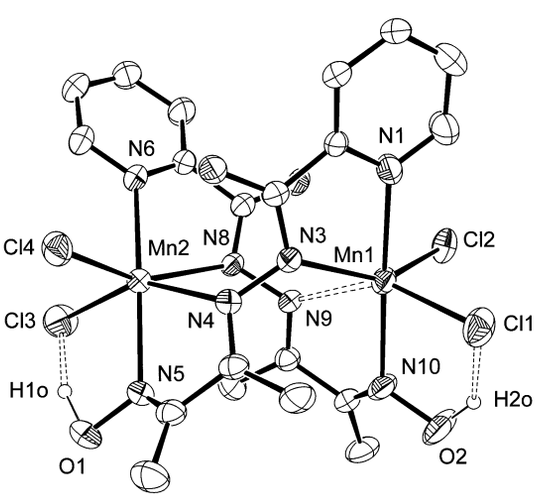

Fig. 1 Structural representation of $[Mn_2(pahox)_2Cl_4]\cdot H_2O$ (**1**·H_2O) (40% probability thermal ellipsoids).

(2.27–2.30 Å) are normal for Mn(II) systems, but Mn(2)–N(4) (2.357(5) Å) and Mn(1)–N(9) (2.464(8) Å) distances are much longer, indicating some possible strain associated with the twisted arrangement. This is illustrated also by a long Mn–Mn distance of 4.821(3) Å, and quite large torsional angles (Mn(1)–N(9)–N(8)–Mn(2) 81.9(5)°, Mn(1)–N(3)–N(4)–Mn(2) 90.6(5)°) around the N–N bridges. The conformation of the complex appears to be locked, as a result of a balance between the equatorial bonding interactions to the diazine nitrogens and two significant hydrogen bonding interactions (Cl(3)–H(1o) 1.895 Å, Cl(1)–H(2o) 2.257 Å), involving the terminal chlorines and the external OH groups on the ligand.

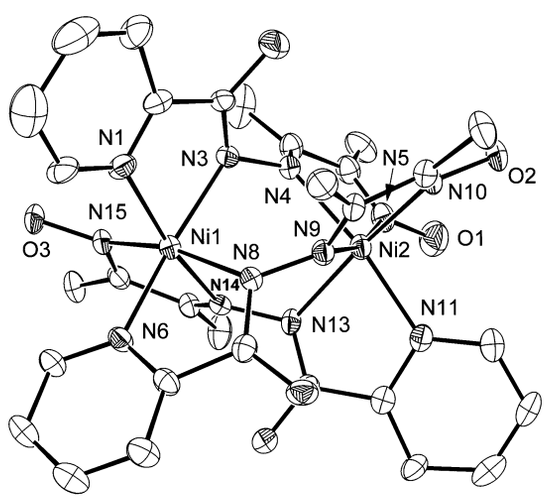

Fig. 2 Structural representation of the dinuclear cation in $[Ni_2(pahox)_3](ClO_4)_4\cdot 4H_2O$ (**2**·$4H_2O$) (40% probability thermal ellipsoids).

Crystal structure of $[Ni_2(pahox)_3](ClO_4)_4\cdot 4H_2O$ (2·$4H_2O$). The structure of the dinuclear cation in **2** is shown in Fig. 2, and selected bond distances and angles are listed in Table 3. The dinuclear cation exists in a spiral-like twisted arrangement with three pahox ligands wrapped around the di-nickel centre, and with three N–N single bonds (N–N 1.380–1.405 Å) acting as bridges. The terminal donors on each ligand are the pyridine and oxime nitrogens, and the oxime OH group remains uncoordinated. The consequence of three bridges compared with the two in **1** is to shorten the metal–metal distance substantially (Ni(1)–Ni(2) 3.654(2) Å). The ligands are arranged asymmetrically with two pointing in one direction. Ni–N distances are substantially shorter than in **1** (<2.1 Å), and normal for Ni(II) complexes of this sort. The incorporation of three ligands causes a more pronounced twist of the dinuclear core. Torsional angles (Ni–N–N–Ni) fall in the range 41–42°,

Table 3 Distances (Å) and angles (°) for **2**

Ni(1)–N(1)	2.060(4)	Ni(2)–N(9)	2.099(3)
Ni(1)–N(3)	2.075(4)	Ni(2)–N(10)	2.064(4)
Ni(1)–N(6)	2.068(4)	Ni(2)–N(11)	2.060(4)
Ni(1)–N(8)	2.066(4)	Ni(2)–N(13)	2.044(4)
Ni(1)–N(14)	2.075(3)	Ni(1)–Ni(2)	3.654(2)
Ni(1)–N(15)	2.072(4)	N(3)–N(4)	1.405(5)
Ni(2)–N(4)	2.077(4)	N(8)–N(9)	1.380(5)
Ni(2)–N(5)	2.081(4)	N(13)–N(14)	1.404(5)
N(1)–Ni(1)–N(3)	77.5(1)	N(4)–Ni(2)–N(5)	75.8(2)
N(1)–Ni(1)–N(6)	98.0(1)	N(4)–Ni(2)–N(9)	90.4(1)
N(1)–Ni(1)–N(8)	94.8(1)	N(4)–Ni(2)–N(10)	94.7(1)
N(1)–Ni(1)–N(14)	168.1(1)	N(4)–Ni(2)–N(11)	168.3(1)
N(1)–Ni(1)–N(15)	99.4(2)	N(4)–Ni(2)–N(13)	92.3(1)
N(3)–Ni(1)–N(6)	168.7(1)	N(5)–Ni(2)–N(9)	165.2(2)
N(3)–Ni(1)–N(8)	91.2(1)	N(5)–Ni(2)–N(10)	99.8(2)
N(3)–Ni(1)–N(14)	91.7(1)	N(5)–Ni(2)–N(11)	98.7(2)
N(3)–Ni(1)–N(15)	95.8(1)	N(5)–Ni(2)–N(13)	94.9(2)
N(6)–Ni(1)–N(8)	78.8(1)	N(9)–Ni(2)–N(10)	75.7(1)
N(6)–Ni(1)–N(14)	93.6(1)	N(9)–Ni(2)–N(11)	95.8(1)
N(6)–Ni(1)–N(15)	95.1(2)	N(9)–Ni(2)–N(13)	90.9(1)
N(8)–Ni(1)–N(14)	90.2(1)	N(10)–Ni(2)–N(11)	96.5(2)
N(8)–Ni(1)–N(15)	165.2(1)	N(10)–Ni(2)–N(13)	164.9(1)
N(14)–Ni(1)–N(15)	76.6(1)	N(11)–Ni(2)–N(13)	77.7(2)

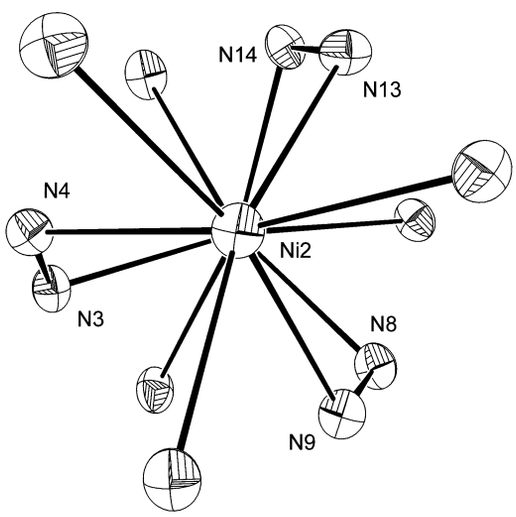

Fig. 3 Core structure in **2**.

with an acute twist of each ligand about the N–N bond (Fig. 3; structural core).

Crystal structure of $[Ni_2(pzhpz)_3](ClO_4)_4\cdot 4H_2O$ ($3\cdot 4H_2O$). The stuctural representation of the dinuclear cation in **3** is shown in Fig. 4, and the core structure in Fig. 5. Selected bond distances and angles are listed in Table 4. Three pzhpz ligands are arranged with a spiral-like twist around the dinickel centre, with a similar structural arrangement to that in **2**. The Ni–Ni separation is 3.739(1) Å, and the Ni–N distances fall in a narrow range (2.055–2.112 Å) typical of Ni(II) in an octahedral geometry. The spiral twist is defined by Ni–N–N–Ni torsional angles in the range 39.8–42.8°, similar to that found in **2**. Complex **4** has a very similar structure (the core structure is shown in Fig. 6; selected bond distances and angles are listed in Table 5), with a Cu–Cu separation of 3.719(1) Å, but quite different Cu–N–N–Cu torsional angles (Cu(1)–N(46)–N(45)–Cu(2) 45.3(5)°, Cu(1)–N(28)–N(27)–Cu(2) 32.3(5)°, Cu(1)–N(9)–N(10)–Cu(2) 43.2(5)°). This results from the tetragonal distortion of the copper(II) centres, with very long axial bonds from Cu(1) to N(28) and N(18) (2.283(1) Å, 2.286(1) Å respectively) and from Cu(2) to N(27) and N(37) (2.301(1) Å, 2.334(1)Å respectively). The equatorial Cu–N distances are much shorter (<2.11 Å). Crystals of **5** were found to be unsuitable for a structural determination, but

Table 4 Distances (Å) and angles (°) for **3**

Ni(1)–N(1)	2.100(2)	Ni(2)–N(13)	2.093(2)
Ni(1)–N(4)	2.075(2)	Ni(2)–N(16)	2.090(2)
Ni(1)–N(9)	2.092(2)	Ni(2)–N(21)	2.085(2)
Ni(1)–N(12)	2.091(2)	Ni(2)–N(24)	2.112(2)
Ni(1)–N(17)	2.096(2)	Ni(1)–Ni(2)	3.739(1)
Ni(1)–N(20)	2.058(2)	N(4)–N(5)	1.413(3)
Ni(2)–N(5)	2.055(2)	N(12)–N(13)	1.423(3)
Ni(2)–N(8)	2.106(2)	N(20)–N(21)	1.419(3)
N(1)–Ni(1)–N(4)	77.23(9)	N(17)–Ni(1)–N(20)	77.33(9)
N(1)–Ni(1)–N(9)	94.66(9)	N(5)–Ni(2)–N(8)	77.32(9)
N(1)–Ni(1)–N(12)	163.86(9)	N(5)–Ni(2)–N(13)	89.03(9)
N(1)–Ni(1)–N(17)	98.54(9)	N(5)–Ni(2)–N(16)	165.46(9)
N(1)–Ni(1)–N(20)	98.02(9)	N(5)–Ni(2)–N(21)	89.45(9)
N(4)–Ni(1)–N(9)	95.24(9)	N(5)–Ni(2)–N(24)	97.46(9)
N(4)–Ni(1)–N(12)	89.19(9)	N(8)–Ni(2)–N(13)	96.65(9)
N(4)–Ni(1)–N(17)	166.15(9)	N(8)–Ni(2)–N(16)	97.88(9)
N(4)–Ni(1)–N(20)	90.11(9)	N(8)–Ni(2)–N(21)	164.72(9)
N(9)–Ni(1)–N(12)	77.74(9)	N(8)–Ni(2)–N(24)	97.24(9)
N(9)–Ni(1)–N(17)	98.27(9)	N(13)–Ni(2)–N(16)	77.81(9)
N(9)–Ni(1)–N(20)	167.06(9)	N(13)–Ni(2)–N(21)	90.66(9)
N(12)–Ni(1)–N(17)	96.64(9)	N(13)–Ni(2)–N(24)	165.67(9)
N(12)–Ni(1)–N(20)	90.60(9)	N(16)–Ni(2)–N(21)	96.77(9)

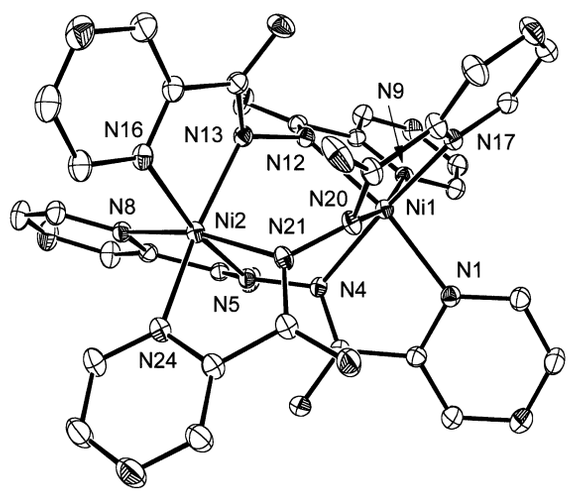

Fig. 4 Structural representation of the dinuclear cation in $[Ni_2(pzhpz)_3](ClO_4)_4\cdot 4H_2O$ ($3\cdot 4H_2O$) (40% probability thermal ellipsoids).

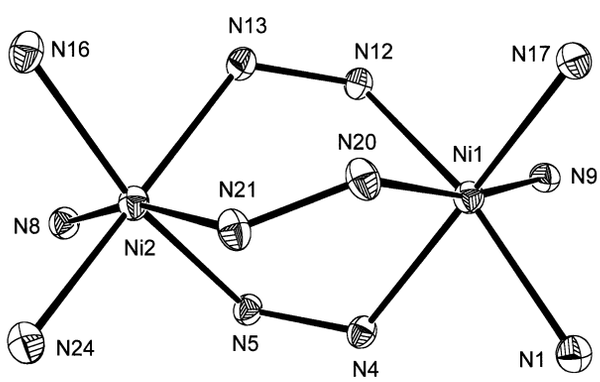

Fig. 5 Core structure in **3**.

spectral and other data (*vide infra*) suggest a spiral tri-ligand structure similar to **4**.

Crystal structure of $[Zn_2(pahap)_3](ZnBr_4)_2\cdot 5H_2O$ ($6\cdot 5H_2O$). The structure of the cation in **6** is shown in Fig. 7, and selected bond distances and angles are listed in Table 6. The dinuclear cation consists of two octahedral Zn(II) centres bridged by three N–N single bonds, with Zn–N distances in the range 2.11–2.20 Å, and with a Zn(1)–Zn(2) separation of 3.881(3) Å. The dinuclear centre dimensions are very close to those observed for

Table 5 Distances (Å) and angles (°) for **4**

Cu(1)–N(10)	2.0330(13)	Cu(2)–N(9)	2.0010(14)
Cu(1)–N(18)	2.2857(15)	Cu(2)–N(19)	2.0767(14)
Cu(1)–N(28)	2.2833(14)	Cu(2)–N(27)	2.3010(13)
Cu(1)–N(36)	2.1029(14)	Cu(2)–N(37)	2.3342(15)
Cu(1)–N(46)	2.0145(14)	Cu(2)–N(45)	2.0417(13)
Cu(1)–N(54)	2.0376(13)	Cu(1)–Cu(2)	3.719(1)
Cu(2)–N(1)	2.0488(13)		
N(10)–Cu(1)–N(18)	75.42(5)	N(1)–Cu(2)–N(9)	79.32(6)
N(10)–Cu(1)–N(28)	92.48(5)	N(1)–Cu(2)–N(19)	98.46(6)
N(10)–Cu(1)–N(36)	94.11(5)	N(1)–Cu(2)–N(27)	95.02(5)
N(10)–Cu(1)–N(46)	89.19(5)	N(1)–Cu(2)–N(37)	97.91(5)
N(10)–Cu(1)–N(54)	166.33(5)	N(1)–Cu(2)–N(45)	164.25(5)
N(18)–Cu(1)–N(28)	161.34(5)	N(9)–Cu(2)–N(19)	163.35(6)
N(18)–Cu(1)–N(36)	91.73(5)	N(9)–Cu(2)–N(27)	88.37(5)
N(18)–Cu(1)–N(46)	102.02(5)	N(9)–Cu(2)–N(37)	102.02(5)
N(18)–Cu(1)–N(54)	99.56(5)	N(9)–Cu(2)–N(45)	88.85(6)
N(28)–Cu(1)–N(36)	74.76(5)	N(19)–Cu(2)–N(27)	75.33(5)
N(28)–Cu(1)–N(46)	91.78(5)	N(19)–Cu(2)–N(37)	94.63(5)
N(28)–Cu(1)–N(54)	95.25(5)	N(19)–Cu(2)–N(45)	95.83(6)
N(36)–Cu(1)–N(46)	166.25(5)	N(27)–Cu(2)–N(37)	164.69(5)
N(36)–Cu(1)–N(54)	98.79(5)	N(27)–Cu(2)–N(45)	94.99(5)
N(46)–Cu(1)–N(54)	79.33(5)	N(37)–Cu(2)–N(45)	74.26(5)

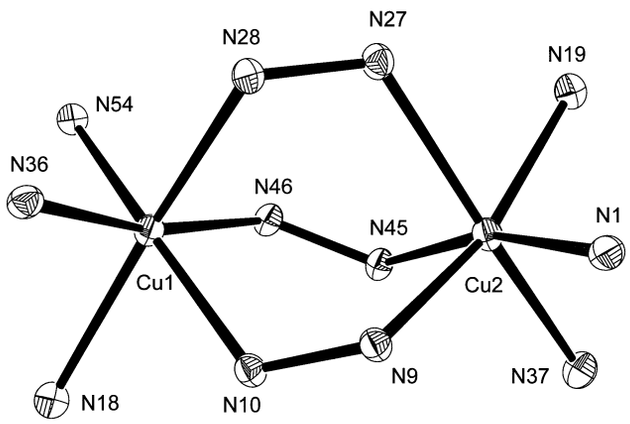

Fig. 6 Core dinuclear structure in $[Cu_2(pzhpz)_3](ClO_4)_4\cdot 5H_2O$ ($\mathbf{4}\cdot 5H_2O$).

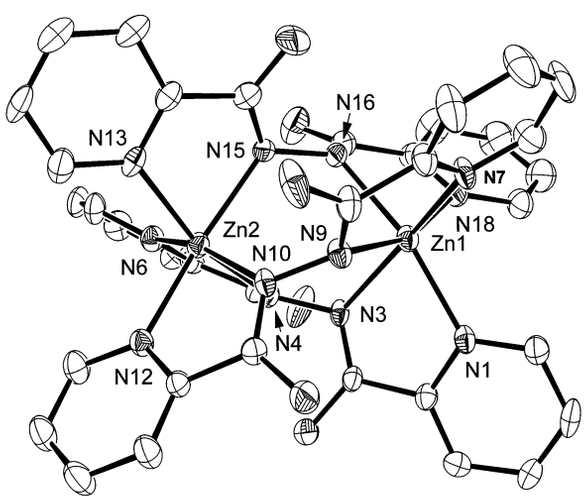

Fig. 7 Structural representation of the dinuclear cation in $[Zn_2(pahap)_3](ZnBr_4)_2\cdot 5H_2O$ ($\mathbf{6}\cdot 5H_2O$) (40% probability thermal ellipsoids).

the Ni(II) and Cu(II) systems, but are slightly smaller than in $[Mn_2(pahap)_3](ClO_4)_4\cdot 5H_2O$.[4] The counter complex anions are non-coordinating tetrahedral $ZnBr_4^{2-}$ ions.

Crystal structure of $[Cd_2(pahap)_2(NO_3)_2(H_2O)_2](NO_3)_2\cdot 4H_2O$ ($\mathbf{7}\cdot 4H_2O$). The structure of the dinuclear Cd(II) cation in **7** is illustrated in Fig. 8, and important bond distances and angles

Table 6 Distances (Å) and angles (°) for **6**

Zn(1)–N(1)	2.140(5)	Zn(2)–N(10)	2.178(6)
Zn(1)–N(3)	2.173(6)	Zn(2)–N(12)	2.193(5)
Zn(1)–N(7)	2.166(7)	Zn(2)–N(13)	2.126(6)
Zn(1)–N(9)	2.151(7)	Zn(2)–N(15)	2.151(5)
Zn(1)–N(16)	2.162(5)	Zn(1)–Zn(2)	3.881(3)
Zn(1)–N(18)	2.144(6)	N(3)–N(4)	1.416(8)
Zn(2)–N(4)	2.113(6)	N(9)–N(10)	1.418(8)
Zn(2)–N(6)	2.192(7)	N(15)–N(16)	1.423(8)
N(1)–Zn(1)–N(3)	74.8(2)	N(4)–Zn(2)–N(6)	75.1(2)
N(1)–Zn(1)–N(7)	102.4(2)	N(4)–Zn(2)–N(10)	88.7(2)
N(1)–Zn(1)–N(9)	98.3(2)	N(4)–Zn(2)–N(12)	98.6(2)
N(1)–Zn(1)–N(16)	161.6(2)	N(4)–Zn(2)–N(13)	162.3(2)
N(1)–Zn(1)–N(18)	99.1(2)	N(4)–Zn(2)–N(15)	88.9(2)
N(3)–Zn(1)–N(7)	162.8(2)	N(6)–Zn(2)–N(10)	162.2(2)
N(3)–Zn(1)–N(9)	88.2(2)	N(6)–Zn(2)–N(12)	100.8(2)
N(3)–Zn(1)–N(16)	88.5(2)	N(6)–Zn(2)–N(13)	98.3(2)
N(3)–Zn(1)–N(18)	99.1(2)	N(6)–Zn(2)–N(15)	98.0(2)
N(7)–Zn(1)–N(9)	75.3(2)	N(10)–Zn(2)–N(12)	73.9(2)
N(7)–Zn(1)–N(16)	95.9(2)	N(10)–Zn(2)–N(13)	99.3(2)
N(7)–Zn(1)–N(18)	98.1(2)	N(10)–Zn(2)–N(15)	89.0(2)
N(9)–Zn(1)–N(16)	88.8(2)	N(12)–Zn(2)–N(13)	98.8(2)
N(9)–Zn(1)–N(18)	162.4(2)	N(12)–Zn(2)–N(15)	161.0(2)
N(16)–Zn(1)–N(18)	75.5(2)	N(13)–Zn(2)–N(15)	75.6(2)

Table 7 Distances (Å) and angles (°) for **7**

Cd(1)–O(1)	2.361(3)	Cd(1)–N(6)	2.317(4)
Cd(1)–O(2)	2.404(3)	O(2)–N(7)	1.255(5)
Cd(1)–N(1)	2.312(4)	N(3)–N(4)	1.442(4)
Cd(1)–N(3)	2.364(3)	Cd(1)–Cd(1′)	4.783(1)
Cd(1)–N(4)	2.369(3)		
O(1)–Cd(1)–O(2)	82.9(1)	O(2)–Cd(1)–N(6)	90.4(1)
O(1)–Cd(1)–N(1)	92.3(1)	N(1)–Cd(1)–N(3)	69.5(1)
O(1)–Cd(1)–N(3)	146.6(1)	N(1)–Cd(1)–N(4)	116.1(1)
O(1)–Cd(1)–N(4)	83.8(1)	N(1)–Cd(1)–N(6)	173.0(1)
O(1)–Cd(1)–N(6)	88.5(1)	N(3)–Cd(1)–N(4)	80.0(1)
O(2)–Cd(1)–N(1)	82.8(1)	N(3)–Cd(1)–N(6)	113.0(1)
O(2)–Cd(1)–N(3)	120.4(1)	N(4)–Cd(1)–N(6)	71.0(1)
O(2)–Cd(1)–N(4)	157.3(1)		

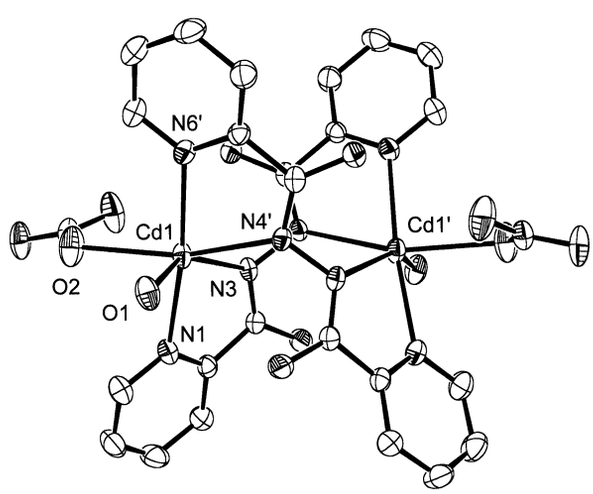

Fig. 8 Structural representation of the dinuclear cation in $[Cd_2(pahap)_2(NO_3)_2(H_2O)_2](NO_3)_2\cdot 4H_2O$ ($\mathbf{7}\cdot 4H_2O$) (40% probability thermal ellipsoids).

are listed in Table 7. The dinuclear unit differs from those in **2–4** and **6** with only two ligands bridging the two metal ions. It is similar to **1** in this respect. Other coordination sites at the octahedral metal centres are occupied by water molecules and monodentate nitrate anionic ligands. The double N–N bridge relaxes the dinuclear centre somewhat, resulting in a long Cd–Cd distance (4.783(1) Å) and large Cd–N–N–Cd torsional angles (88.2(4)°). These dimensions compare closely with those in **1**.

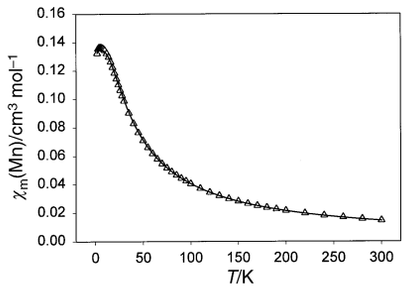

Fig. 9 Variable temperature magnetic data for $[Mn_2(pahox)_2Cl_4]\cdot H_2O$ (**1**·H_2O). The solid line was calculated with $g = 2.035(4)$, $J = -1.4(1)$ cm^{-1}, $\theta = 0.6$ K, $\rho = 0.0051$, $N\alpha = 18 \times 10^{-6}$ cm^3 mol^{-1} (Mn) ($10^2R = 0.46$; $R = [\Sigma(\chi_{obs.} - \chi_{calc.})^2/\Sigma\chi_{obs.}^2]^{1/2}$).

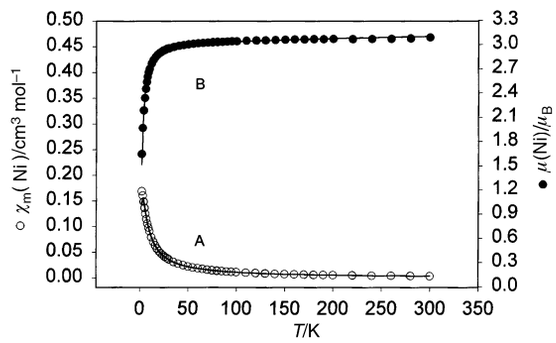

Fig. 10 Variable temperature magnetic data for $[Ni_2(pahox)_3](ClO_4)_4\cdot 4H_2O$ (**2**·$4H_2O$). The solid line (B) was calculated with $g = 2.168(4)$, $J = -0.77(1)$ cm^{-1}, $zJ' = -0.36$ cm^{-1}, $D = -0.57$ cm^{-1}, $\rho = 0.002$, $N\alpha = 180 \times 10^{-6}$ cm^3 mol^{-1} (Ni) ($10^2R = 1.0$; $R = [\Sigma(\chi_{obs.} - \chi_{calc.})^2/\Sigma\chi_{obs.}^2]^{1/2}$).

Complex self-assembly

Bis-bidentate ligands like pahap, pzhpz and pahox have two coordination pockets capable of binding two metals, and in cases where potential co-ligands (*e.g.* Cl, Br, acac, bipy, glycinate, alaninate *etc.*,)[1–4] are present ligand competition produces dinuclear mono-ligand complexes. In the absence of such co-ligands the coordination requirements of the metals are met by a suitable arrangement of multiples of the available bis-bidentate ligands to form a homoleptic system, by a self-assembly process. It would be reasonable to assume that mono-nuclear subunits with one or two ligands bound at their bidentate ends would be precursor fragments in the self-assembly process. It is clear that in **1** chlorine is a good co-ligand, occupying two sites per metal, and thus leaves space for two main ligands only. With weakly coordinating perchlorate anions there is no significant co-ligand competition and the coordination requirements of the two metals are met by a combination of three ligands per two metal units (*e.g.* **2**). The formation of a 2 : 2 (M : L) structure in **7**, with bound monodentate nitrates, indicates the competitive nature of a ligand with stronger donor properties. The significant molecular twisting of the 2 : 3 (M : L) systems is largely a flexible response of the complex to steric constraints associated with the NH_2 and CH_3 groups attached to the diazine N–N framework of the ligands, and the geometric requirements of the two six-coordinate pseudo-octahedral metal ion centres. The rotationally flexible N–N bonds allow the ligands to twist freely to minimize these steric interactions. In **1** it is apparent that some degree of restraint is imposed by the hydrogen bonding interactions (*vide supra*).

Magnetic properties

Variable temperature magnetic susceptibility data for **1** (Fig. 9) show a maximum at 10 K, typical of a system exhibiting intramolecular antiferromagnetic exchange. Fitting of the data to the standard isotropic exchange expression for two $S = 5/2$ centres ($H = -2JS_1\cdot S_2$) gave an excellent result with $g = 2.035(4)$, $J = -1.4(1)$ cm^{-1}, $\theta = 0.6$ K, $\rho = 0.0051$, $N\alpha = 18 \times 10^{-6}$ cm^3 mol^{-1} ($10^2R = 0.46$; $R = [\Sigma(\chi_{obs.} - \chi_{calc.})^2/\Sigma\chi_{obs.}^2]^{1/2}$; solid line in Fig. 9 calculated with these parameters; ρ is the fraction of Curie-like paramagnetic impurity, $N\alpha$ is temperature independent paramagnetism, θ is a Weiss-like temperature correction). These data contrast markedly with the results for $[Mn_2(pahap)_3](ClO_4)_4\cdot 5H_2O$,[4] which exhibits intramolecular ferromagnetic coupling, and can be directly associated with the twisting effect of the manganese magnetic orbitals relative to the orientation of the p orbitals of the N–N bridges.[1–3] The Mn–N–N–Mn torsional angles in **1** (81.9°, 90.6°) are much larger than those in $[Mn_2(pahap)_3](ClO_4)_4\cdot 5H_2O$. (44.2° ave.). The opening of the dinuclear centre, as a result of the presence of just two ligands, and the OH–Cl hydrogen bonding constraints, allows the system to enter the antiferromagnetic realm for this kind of bridge, in complete agreement with earlier results.[1–3]

Complex **2** shows antiferromagnetic behaviour also, with a magnetic moment (per Ni) dropping form 3.1 μ_B at 300 K to 1.6 μ_B at 2 K (Fig. 10). The data were fitted initially to a simple isotropic exchange expression for two $S = 1$ centres ($H = -2JS_1\cdot S_2$), and a small negative J value was obtained ($g = 2.15(1)$, $J = -0.99(5)$ cm^{-1}, $\rho = 0.001$, $N\alpha = 90 \times 10^{-6}$ cm^3 mol^{-1}; Fig. 10(A)). Given that this small $|J|$ value could be comparable with zero field splitting for the octahedral nickel(II) centre, an expanded expression (eqns. (1)–(3)) including zero field splitting (D), intermolecular exchange (zJ') and paramagnetic impurity fraction (ρ) was attempted.[15]

$$\chi = \frac{Ng^2\beta^2F(J,T)}{[kT - 4zJ'F(J,T)]} + N\alpha \quad (1)$$

$$F(J,T) = \frac{1 + 5e^{4J/kT}}{3 + 5e^{4J/kT} + e^{-2J/kT}} \quad (2)$$

$$H_o = -2J\hat{s}_1\cdot\hat{s}_2 - D(\hat{s}_{1z}^2 + \hat{s}_{2z}^2) \quad (3)$$

A good data fit was found for $g = 2.168(4)$, $J = -0.77(1)$ cm^{-1}, $zJ' = -0.36$ cm^{-1}, $D = -0.57$ cm^{-1}, $\rho = 0.002$, $N\alpha = 180 \times 10^{-6}$ cm^3 mol^{-1} (Ni), ($10^2R = 1.0$). The solid line in Fig. 10(B) was calculated with these parameters. The very weak antiferromagnetic coupling in this compound is perhaps not surprising given the small Ni–N–N–Ni torsional angles (41–42°). These are comparable with $[Mn_2(pahap)_3](ClO_4)_4\cdot 5H_2O$ (torsional angle = 44.2°),[4] which exhibits weak ferromagnetic coupling. It would seem reasonable that there would be a slightly different angle range for the crossover from ferromagnetic to antiferromagnetic behaviour for comparable compounds with different ligands and different metals.

Complex **3** shows an essentially constant moment of 3.0 μ_B per metal from 300–5 K, followed by a very slight drop at lower temperature. This behaviour is indicative of no coupling between the Ni centres and is again consistent with the small Ni–N–N–Ni torsional angle (41.3° ave.). Despite the structural similarity with **2**, the change in ligand would inevitably influence the exchange situation, but it is clear that the magnetic difference between these compounds is small.

In contrast **4** shows a temperature dependence of magnetic moment (Fig. 11) typical of a system exhibiting significant intramolecular ferromagnetic exchange. μ rises from about 1.88 μ_B (per Cu) in the range 300–100 K to 2.08 μ_B at 4 K. The variable temperature data were fitted to the Bleaney–Bowers equation[16] and a very good fit gave $g = 2.11(1)$, $J = 6.6(1)$ cm^{-1}, $\theta = -0.12$ K, $\rho = 0.013$, $N\alpha = 60 \times 10^{-6}$ cm^3 mol^{-1} (Cu) ($10^2R = 0.3$) (Fig. 11; solid line). The very slight drop in moment between 300 K and ≈170 K is associated with the presence of a very small antiferromagnetic component,

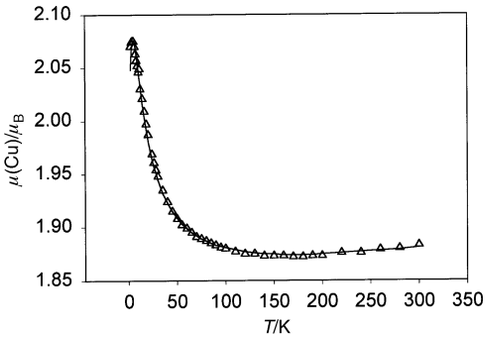

Fig. 11 Variable temperature magnetic data for $[Cu_2(pzhpz)_3](ClO_4)_4 \cdot 5H_2O$ (**4**·$5H_2O$). The solid line was calculated with $g = 2.11(1)$, $J = 6.6(1)$ cm^{-1}, $\theta = -0.12$ K, $\rho = 0.013$, $N\alpha = 60 \times 10^{-6}$ cm^3 mol^{-1} (Cu) ($10^2R = 0.3$; $R = [\Sigma(\chi_{obs.} - \chi_{calc.})^2/\Sigma\chi_{obs.}^2]^{1/2}$).

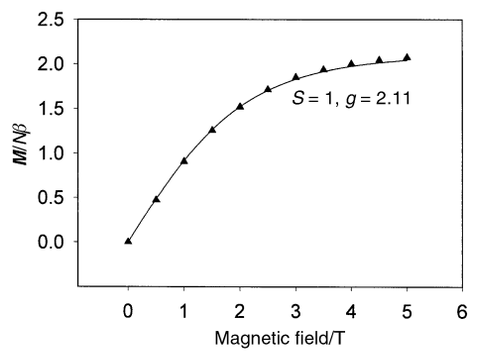

Fig. 12 Magnetization data as a function of field (0–5 T) at 2 K for $[Cu_2(pzhpz)_3](ClO_4)_4 \cdot 5H_2O$ (**4**·$5H_2O$). The solid line was calculated from the Brillouin function for an $S = 2/2$ system with $g = 2.11$.

probably intermolecular in nature, revealed in the fitting by the inclusion of a small negative θ correction. Magnetization data obtained at 2 K at variable field up to 5 T (Fig. 12) show almost complete saturation at 5 T, and a saturation value of 1.99 $N\beta$ corresponding to a $S = 1$ ground state (Fig. 12; solid line from the theoretical Brillouin function for $g = 2.11$ and $S = 1$). An examination of the core structure of **4** (Fig. 6) shows that the magnetic planes of the two copper atoms are defined by Cu(1) and N(10), N(36), N(54) and N(46) and Cu(2) and N(1), N(9), N(45) and N(19) (short in plane contacts), which leads to just two diazine bridge groups that could possibly be involved in contributing to antiferromagnetic exchange (N(45)–N(46) and N(9)–N(10)). Cu–N–N–Cu torsional angles are small overall (<46°), and so ferromagnetic coupling would be expected. The angles between the copper magnetic planes at Cu(1) and Cu(2) can be estimated from the relative orientation of the Cu–N–C–C–N chelate rings defined by the N_2 donor ends of each ligand, in order to compare this compound directly with previously reported examples.[2] This acute angle of 66.4° compares with those observed previously, where at angles ~80° ferromagnetic coupling would be expected.[2] A similar profile of magnetic moment versus temperature was observed for **5** and the data were fitted to the Bleaney–Bowers equation to give $g = 2.107(1)$, $J = 7.3(1)$ cm^{-1}, $\rho = 0.0005$, $\theta = -0.18$ K, TIP = 50×10^{-6} cm^3 mol^{-1} (Cu) ($10^2R = 0.41$), consistent with the anticipated spiral structural arrangement, with three pahap ligands bound to two copper(II) centres, in a similar manner to **4**. Magnetization data at 2 K in the range 0–5 T again confirm an $S = 1$ ground state.

Conclusion

New spiral dinuclear complexes with N_4 bis-bidentate ligands with rotationally flexible N–N single bond bridges are reported. The stoichiometric outcome *i.e.* 2 : 2 or 3 : 2 ligand : metal ratio, depends on the presence of competitive ligating anionic groups, and chlorine and nitrate have been shown to act as ligands, while perchlorate does not. Examples with both antiferromagnetic and ferromagnetic behaviour are found, with the primary rationale for the sign of magnetic exchange interaction being the angle of rotation of the metal magnetic orbitals relative to the N–N single bond bridge.

Acknowledgements

We thank NSERC (Canada) and EPSRC (UK) for financial support, Dr. J. N. Bridson for stuctural data on **1**, and Dr. R. McDonald, University of Alberta, for structural data on **3**.

References

1 Z. Xu, L. K. Thompson and D. O. Miller, *Inorg. Chem.*, 1997, **36**, 3985 and references therein.
2 L. K. Thompson, Z. Xu, A. E. Goeta, J. A. K. Howard, H. J. Clase and D. O. Miller, *Inorg. Chem.*, 1998, **37**, 3217.
3 Z. Xu, L. K. Thompson, C. J. Matthews, D. O. Miller, A. E. Goeta, C. Wilson, J. A. K. Howard, M. Ohba and H. Ōkawa, *J. Chem. Soc., Dalton Trans.*, 2000, 69.
4 Z. Xu, L. K. Thompson, D. O. Miller, H. J. Clase, J. A. K. Howard and A. E. Goeta, *Inorg. Chem.*, 1998, **37**, 3620.
5 D. S. Brown, V. H. Crawford, J. W. Hall and W. E. Hatfield, *J. Phys. Chem.*, 1977, **81**, 1303.
6 SIR92: A. Altomare, M. Cascarano, C. Giacovazzo and A. Guagliardi, *J. Appl. Crystallogr.*, 1993, **26**, 343.
7 DIRDIF94: P. T. Beurskens, G. Admiraal, G. Beurskens, W. P. Bosman, R. de Gelder, R. Israel and J. M. M. Smits, The DIRDIF-94 program system, Technical Report of the Crystallography Laboratory, University of Nijmegen, The Netherlands.
8 D. T. Cromer and J. T. Waber, *International Tables for X-Ray Crystallography*, vol. IV, The Kynoch Press, Birmingham, England, 1974, Table 2.2 A.
9 J. A. Ibers and W. C. Hamilton, *Acta Crystallogr.*, 1964, **17**, 781.
10 D. C. Creagh and W. J. McAuley, *International Tables for Crystallography*, vol. C, ed. A. J. C. Wilson, Kluwer Academic Publishers, Boston, 1992, Table 4.2.6.8, pp. 219–222.
11 teXsan for Windows: Crystal Structure Analysis Package, Molecular Structure Corporation, Houston, TX, 1997.
12 J. Cosier and A. M. Glazer, *J. Appl. Crystallogr.*, 1986, **19**, 105.
13 (*a*) Siemens SMART Data Collection Software, version 4.050, Siemens Analytical X-Ray Instruments Inc., Madison, WI, 1996; (*b*) Siemens SAINT Data Reduction Software, version 4.050, Siemens Analytical X-Ray Instruments Inc., Madison, WI, 1996.
14 G. M. Sheldrick, SHELXTL 5.04/VMS, An integrated system for solving, refining and displaying crystal structures from diffraction data, Siemens Analytical X-Ray Instruments Inc., Madison, WI, 1995.
15 A. P. Ginsberg, R. L. Martin, R. W. Brookes and R. C. Sherwood, *Inorg. Chem.*, 1972, **11**, 2884.
16 B. Bleaney and K.D. Bowers, *Proc. R. Soc. London, Ser. A*, 1952, **214**, 451.